N 62 10216

Technical Report No. 32-186

A Limit Analysis of the Collapse of Hexagonal Cell Structures Under Axial Load

R. K. McFarland, Jr.

jpl

JET PROPULSION LABORATORY
CALIFORNIA INSTITUTE OF TECHNOLOGY
PASADENA, CALIFORNIA

December 1, 1961

NATIONAL AERONAUTICS AND SPACE ADMINISTRATION
CONTRACT NO. NASW-6

Technical Report No. 32-186

A Limit Analysis of the Collapse of Hexagonal Cell Structures Under Axial Load

R. K. McFarland, Jr.

Charles W Cole for
R. R. McDonald, *Chief*
Engineering Research

JET PROPULSION LABORATORY
CALIFORNIA INSTITUTE OF TECHNOLOGY
PASADENA, CALIFORNIA

December 1, 1961

Copyright © 1961
Jet Propulsion Laboratory
California Institute of Technology

CONTENTS

I. Introduction 1

II. Energy of Deformation 1

III. Energy of Bending Deformation 5

IV. Energy of Shear Deformation 9

V. Discussion of Results 11

VI. Experimental Results 12

VII. Conclusion 14

Nomenclature 14

Appendix: Test Procedures 15

Bibliography 17

FIGURES

1. Views of fully crushed hexagonal cell structure 2

2. Isometric projection of idealized mode of collapse of cell structure . . . 3

3. Occurrence of in-plane shear deformation during crushing of hexagonal cell element 4

4. Horizontal projection of partially rotated basic panel 5

5. Horizontal projection of cell structure 6

6. Panel element rotations during crushing of hexagonal cell structure . . . 7

7. Cross section of hexagonal cell structure illustrating area tributary to two basic panel elements 8

8. Exploded view of cell model indicating forces causing in-plane deformation 9

9. Shear mechanism and corresponding parameters 10

10. Crushing stress vs. t/S for 3003 H-19 aluminum hexagonal cell structure 11

Page intentionally left blank

FIGURES (Cont'd)

11. Crushing stress vs. *t*/*S* for 3003 H-19 aluminum hexagonal cell structure 12

12. Crushing stress vs. *t*/*S* for 5052 H-39 aluminum hexagonal cell structure 12

13. Views of partially crushed hexagonal cell structure showing shear failure 13

A-1. Hexagonal cell structure prior to testing 15

A-2. Load-deflection curve for 3003 H-19 aluminum hexagonal cell structure loaded statically 15

ABSTRACT

A method is presented for determining the approximate crushing stress of hexagonal cell structures subjected to axial loading. The purpose of performing this analysis was to determine an approximate analytical relation which can be used to compute the crushing stress of a given hexagonal cell structure. Of additional importance was the determination of the parameters that control the crushing stress and the sensitivity of the crushing stress to variations in these parameters. Experimental verification which was obtained for the resulting relations indicates that this method of analysis provides very effective upper and lower limits on the mean crushing stress of hexagonal cell structures.

I. INTRODUCTION

This Report presents an upper-bound limit analysis of hexagonal cell structures subject to axial loading. The analysis is an approximate one, assuming a rigid-plastic material with equal yield stress in tension and compression, and neglecting the effect of superimposed axial stresses on the yield criterion.

A simple mode of collapse for the hexagonal cell structure is assumed, based on experimental observations, and from this the collapse mechanisms are determined. The limit analysis techniques are then applied to the collapse mechanisms, and the energy of deformation is computed. The energy of deformation is then equated to the change in potential energy of the applied force, and from this, a crushing force per unit area is obtained. The availability of these analytical relations allows a rational evaluation to be made of the efficiency of hexagonal cell structures as energy absorbers.

II. ENERGY OF DEFORMATION

On close examination of a crushed hexagonal cell structure, it is found that there is a definite symmetry to the collapse mode and that the collapse geometry is reproducible, as shown in Fig. 1. Unlike a thin cylindrical shell loaded axially, the collapse mode of the hexagonal cell is a function of the cell shape and geometrical constraints, and does not change with variations of the cell-diameter to wall-thickness ratio for the range of this ratio considered in this analysis.

Once the basic mode of collapse is resolved, the mechanisms of collapse can be determined. By performing a limit analysis on the collapse mechanisms, the parameters that govern the collapse strength can be derived and expressed rationally.

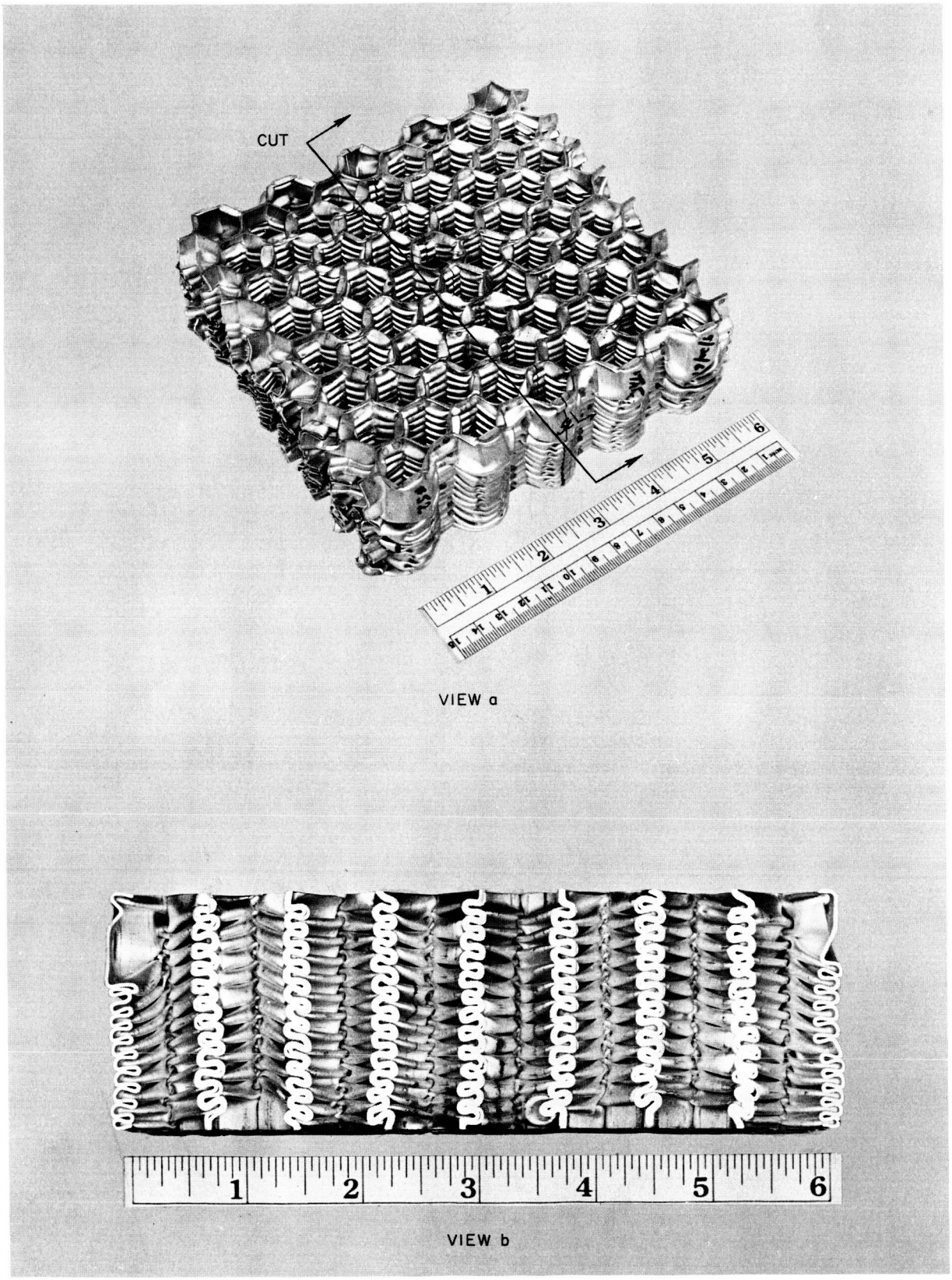

Fig. 1. Views of fully crushed hexagonal structure

To determine the crushing strength of the basic mode of collapse, an idealized model of this mode, shown in Fig. 2, was determined from experimental observation. It will be noted from Fig. 2 that the mode is symmetrical with respect to plate elements taken from the cellular structure. Because of geometrical constraints induced by adjoining cells in the complete cellular array, this mode is different from the mode that would be obtained from an individual hexagonal cell loaded axially.

Considering the collapse mechanisms of the idealized model, it is apparent that in addition to the formation of a hinge mechanism along the fold lines, an in-plane deformation will have to occur to allow the model to collapse further. The need for this deformation is clarified in Fig. 3. In this cell element, the angle γ remains constant during crushing. For this deformation to continue, the angle γ would have to decrease or the angle ψ increase. The angle ψ can increase either by an in-plane shear deformation occurring in the panel elements or a plastic rolling action occurring normal to and along the diagonal hinges. It is assumed that this action is accommodated by in-plane shear deformation; however, as will be discussed in Part IV, a certain amount of the plastic rolling deformation must occur with the shear deformation to obtain compatible deflections of the basic panel elements.

On the basis of these assumptions, limit analyses were performed for a bending mechanism and a shear mechanism.

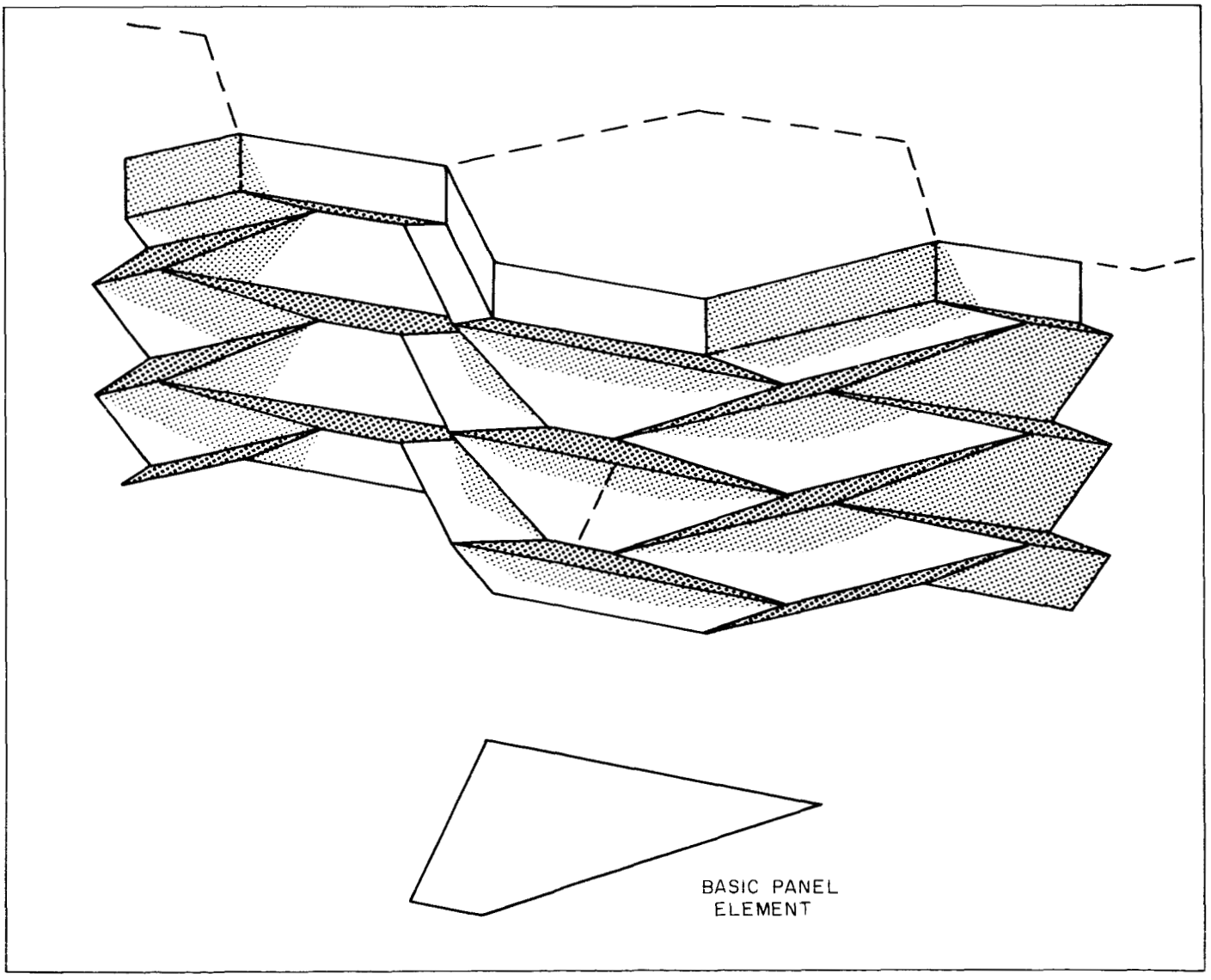

Fig. 2. Isometric projection of idealized mode of collapse of cell structure

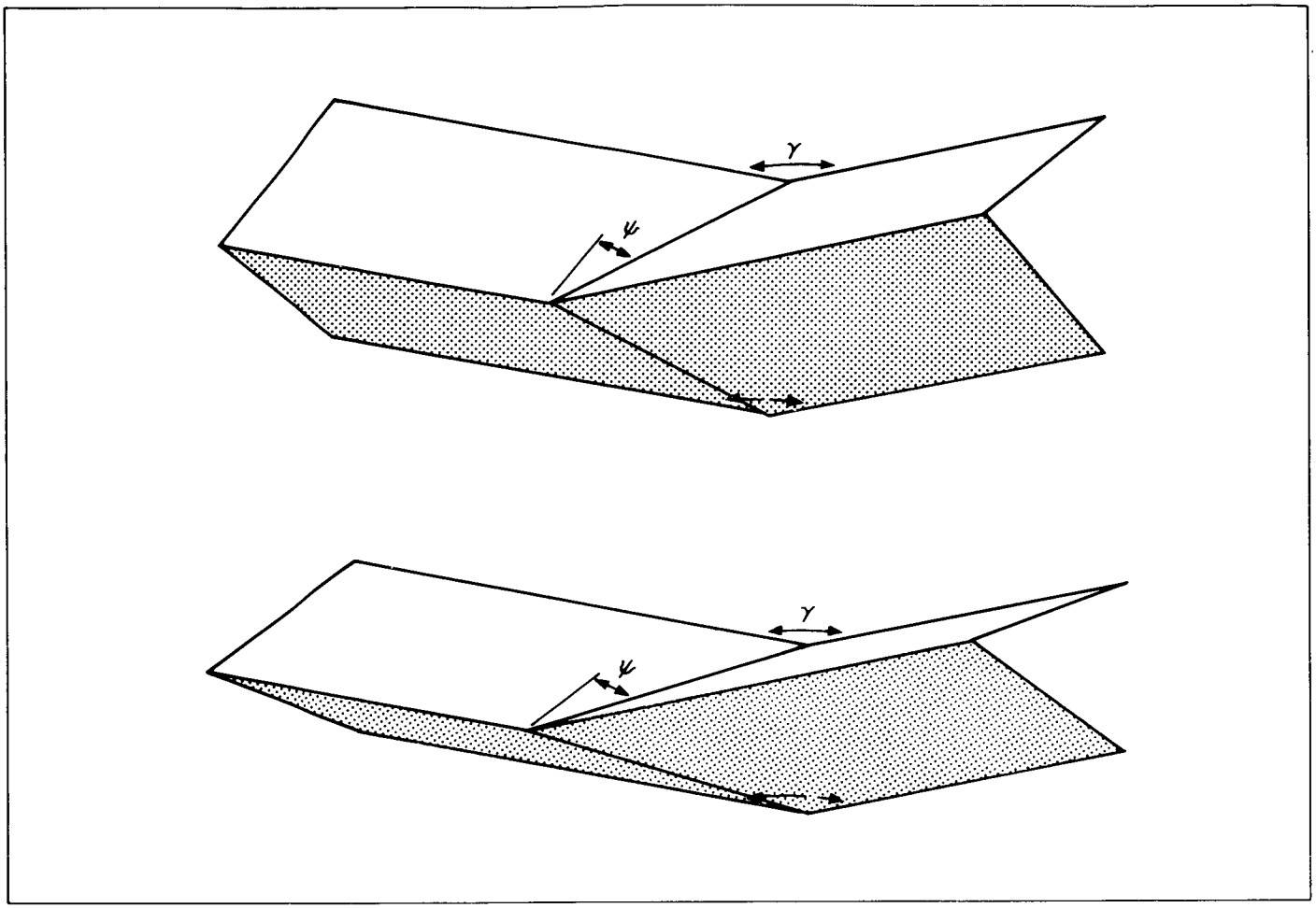

Fig. 3. Occurrence of in-plane shear deformation during crushing of hexagonal cell element

III. ENERGY OF BENDING DEFORMATION

To perform a limit analysis on the bending mechanism, the idealized model is divided into identical basic elements, as shown in Fig. 2, 4, and 5. The energy of deformation incurred by one of the basic elements during the collapse of the model will be determined and the results applied to the composite model. It is necessary to define several relationships. Referring to Fig. 5,

$$D = \frac{S}{\sqrt{3}} \tag{1}$$

$$A = \tfrac{1}{2}\,(D - \sqrt{3}\,P_w \sin\theta) \tag{2}$$

$$B_t = \frac{P_w}{2}\,(1 + 3\sin^2\theta)^{1/2} \tag{3}$$

$$\text{and letting } \beta = (1 + 3\sin^2\theta)^{1/2} \tag{3a}$$

$$B_t = \frac{P_w\,\beta}{2} \tag{4}$$

$$K = \frac{P_w}{D} \tag{5}$$

Note from Fig. 4 that for an increment of deformation, two sides of the basic element rotate through an angle $\Delta\theta$, but the diagonal side will rotate through an angle $\Delta\phi$, for the same deformation. From Fig. 4, the relation between these two angles is

$$\tan\theta = \frac{2}{\sqrt{3}}\tan\theta \tag{6}$$

and

$$\frac{d\phi}{d\theta} = \frac{\sqrt{3}}{2}\,\frac{\cos^2\phi}{\cos^2\theta} \tag{7}$$

Formulating the expression for the energy of bending deformation, let

$$dU_1 = M\Delta\theta$$

Then

$$M\Delta\theta = AM_{yp}\,\Delta\theta + [A + 2\,B\cos(\pi/6)]\,\Delta\theta + 2\,B_t\,\Delta\phi \tag{8}$$

Substituting Eq. (1) through (7) into Eq. (8),

$$M\Delta\theta = \frac{S}{\sqrt{3}}M_{yp}\left[1 + \frac{\sqrt{3}}{2}K\beta\frac{\cos^2\phi}{\cos^2\theta}\right]\Delta\theta \tag{9}$$

To facilitate the integration of this expression, transform the variables $\Delta\theta$, ϕ and θ to $\Delta\psi$ and ψ. From Fig. 5,

$$\cos\psi = P_w/2B_t$$

Using Eq. (4),

$$\cos\psi = \frac{1}{\beta} = \frac{1}{(1 + 3\sin^2\theta)^{1/2}} \text{ or } \sin\theta = \pm\frac{1}{\sqrt{3}}\tan\psi$$

Since ψ increases as θ increases,

$$\sin\theta = \frac{1}{\sqrt{3}}\tan\psi \tag{10}$$

and from this relation,

$$\cos^2\theta = \frac{3 - \tan^2\psi}{3} \tag{11}$$

and

$$d\theta = \frac{\sec^2\psi\,d\psi}{(3 - \tan^2\psi)^{1/2}} \tag{12}$$

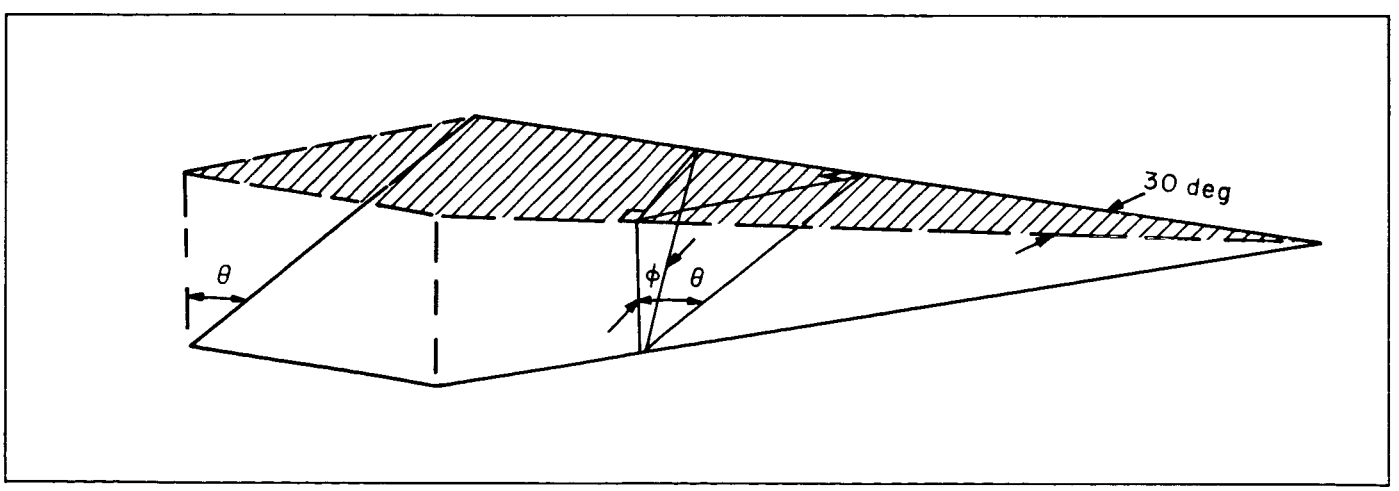

Fig. 4. Horizontal projection of partially rotated basic panel

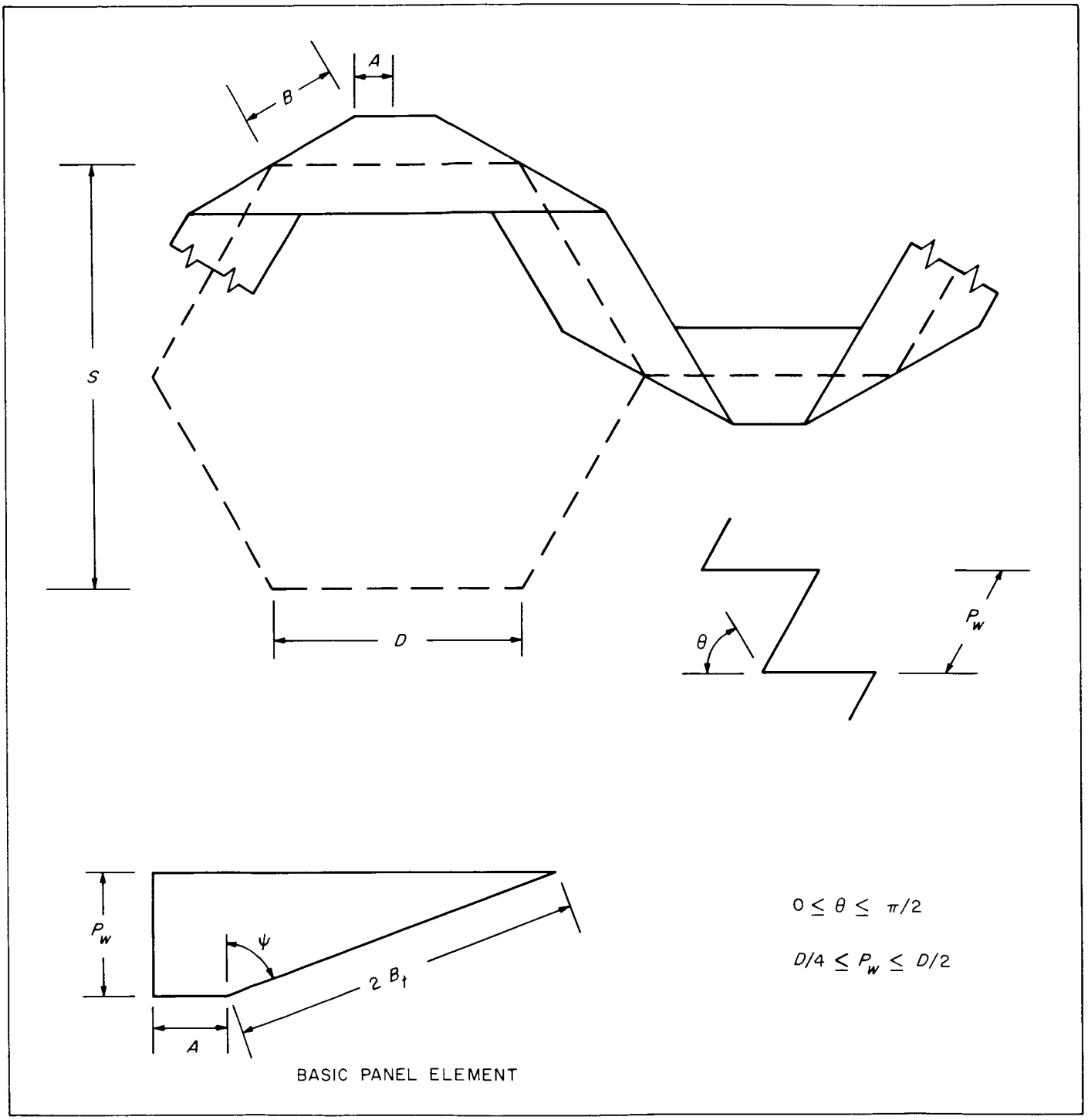

Fig. 5. Horizontal projection of cell structure

Restating Eq. (6),

$$\tan\phi = \frac{\sqrt{3}}{2}\tan\theta = \frac{\sqrt{3}}{2}\frac{\sin\theta}{\cos\theta} \qquad (12a)$$

Substituting Eq. (10) and (11) in Eq. (12a),

$$\tan\phi = \frac{\sqrt{3}\tan\psi}{2\,(3 - \tan^2\psi)^{1/2}} \qquad (13)$$

and from Eq. (13),

$$\cos^2\phi = \frac{4\,(3 - \tan^2\psi)}{12 - \tan^2\psi} \tag{14}$$

Substituting the relations expressed in Eq. (11), (12), and (14) into Eq. (9),

$$dU_1 = M\Delta\theta = \frac{S}{\sqrt{3}} M_{yp}\left[\frac{12\cos\psi - \tan^2\psi\cos\psi + 6\sqrt{3}K}{(13\cos^2\psi - 1)\ (4\cos^2\psi - 1)^{1/2}}\right] d\psi \tag{15}$$

Writing Eq. (15) in integral form,

$$U_1 = \frac{S}{\sqrt{3}} M_{yp}\left\{\int_{\psi_1}^{\psi_2} \frac{12\cos\psi\, d\psi}{(13\cos^2\psi - 1)\ (4\cos^2\psi - 1)^{1/2}} - \int_{\psi_1}^{\psi_2} \frac{\tan^2\psi\cos\psi\, d\psi}{(13\cos^2\psi - 1)\ (4\cos^2\psi - 1)^{1/2}} + 6\sqrt{3}K\int_{\psi_1}^{\psi_2} \frac{d\psi}{(13\cos^2\psi - 1)\,(4\cos^2\psi - 1)^{1/2}}\right\}$$

In terms of the limits of integration ψ_1 and ψ_2, the integrated result is

$$U_1 = \frac{S}{\sqrt{3}} M_{yp}\left\{1.1547\tan^{-1}\frac{0.866\sin\psi}{(4\cos^2\psi - 1)^{1/2}} + \tan^{-1}\frac{(4\cos^2\psi - 1)^{1/2}}{\sin\psi} - \frac{2}{\sqrt{3}}\tan^{-1}\frac{2\,(4\cos^2\psi - 1)^{1/2}}{\sqrt{3}\sin\psi} - 4\sqrt{3}K\left[-\frac{3}{4}\mathcal{F}\left(\phi, \frac{\sqrt{3}}{2}\right) + \frac{13}{12}\Pi\left(\phi, \frac{1}{3}\frac{\sqrt{3}}{2}\right)\right]_{\psi_1}^{\psi_2}\right\} \tag{16}$$

where $\mathcal{F}$ and Π refer to elliptic integrals of the first and third kind, respectively.

To establish the limits of integration for Eq. (16), it is necessary to consider the process of collapse of a hexagonal cell section. If an axial cut is taken through the wall of a partially collapsed cell unit, it is noted that only two basic panel elements will be subject to rotation at any given time, as illustrated in Fig. 6.

In collapsing a depth of P_w, Panel 1 rotates from $\theta = 0$ deg to $\theta = 30$ deg. Panel 2 rotates from $\theta = 30$ deg to $\theta = 90$ deg. In terms of ψ, these limits would be:

Panel 1: $\psi = 0$ deg to $\psi = 40.89$ deg

Panel 2: $\psi = 40.89$ deg to $\psi = 60$ deg

The integration could be performed in one operation; however, for later reference, the integration will be performed for each panel element.

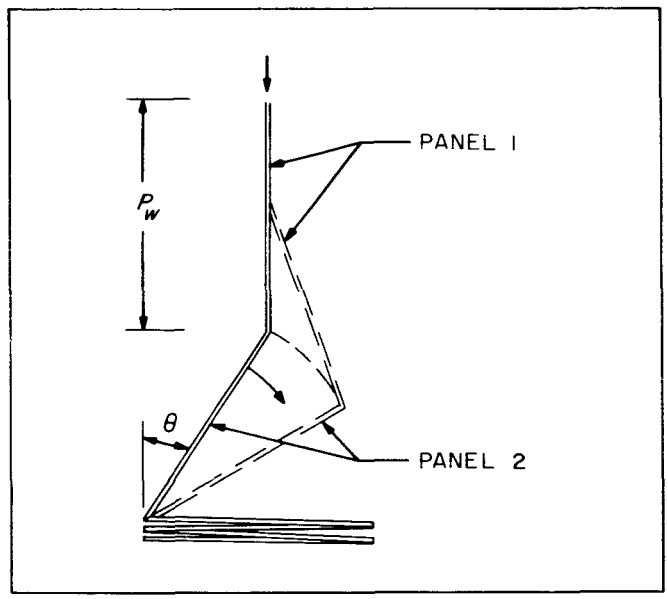

Fig. 6. Panel element rotations during crushing of hexagonal cell structure

Evaluating Eq. (16) with the above limits of integration,

$$U_1 = \frac{S}{\sqrt{3}} M_{yp}\left\{\left[0.547 + 8.016\,K\right] + \left[1.509 + 4.381\,K\right]\right\}$$

where the two sets of brackets refer to Panels 1 and 2, respectively.

Writing the combined results

$$U_1 = \frac{S}{\sqrt{3}} M_{yp}\left[\,2.057 + 12.396\,K\,\right] \tag{17}$$

This energy expression is equal to the mean crushing force times the distance over which it acts. To convert this to the mean crushing stress, it is necessary to determine the contributing area. Fig. 7 represents a portion of a hexagonal cell structure.

As shown, two of the walls of each cell are of double thickness. This fact was not taken into consideration in the evaluation of the energy of deformation. It was as-

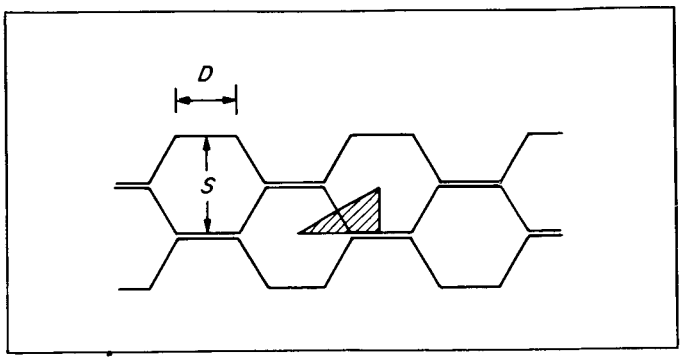

Fig. 7. Cross section of hexagonal cell structure illustrating area tributary to two basic panel elements

sumed that there was no shear transfer between these walls during bending. The contributing area of two basic panel elements is

$$\frac{3\sqrt{3}}{8} D^2$$

Recalling from conventional limit theory that the plastic hinge moment may be written in terms of the yield stress as

$$M_{yp} = \frac{t^2}{4} \sigma_{yp}$$

the above two expressions may be substituted into Eq. (17) to obtain the mean crushing stress

$$F = \frac{4}{\sqrt{3}} \frac{\sigma_{yp}}{K} \frac{t^2}{S^2} \left[2.057 + 12.396\, K \right]$$

or

$$F = \frac{\sigma_{yp}}{K} \frac{t^2}{S^2} \left[4.750 + 28.628\, K \right] \qquad (18)$$

IV. ENERGY OF SHEAR DEFORMATION

The limit analysis for the shear mechanism will be performed in the same manner used to determine the energy of bending deformation.

It is necessary to determine the distribution of forces in the structure that produce in-plane deformations. Fig. 8 is an exploded view of a partially crushed hexagonal cell section and indicates the most probable distribution of forces that exist due to axial loading. The forces are represented as point loads to simplify the visualization of their distribution in the structure. As noted in Fig. 8, the skewed side panels are subjected to a loading that would tend to induce in-plane shear deformations. The center panels are loaded in such a manner that no shear action could result from this loading condition. To maintain geometrical compatibility, if the side panels shear, the center panels must also change shape to conform to the new geometry. At this point, it is necessary to consider a refinement of the idealized model. In an actual specimen, as shown in Fig. 1, there are no sharp re-entrant angles and no ideal plastic hinges. At the intersections of the basic panel elements, relatively large radius bends and regions of plastically deformed material occur. Therefore, it is assumed that the incompatibility in geometry mentioned above will be satisfied by the complex deformations that occur in an actual specimen, and that shearing deformation will occur only in the side panels. The validity of this assumption is justified by experimental confirmation and a consideration of the force distribution on the center panels, as shown in Fig. 8.

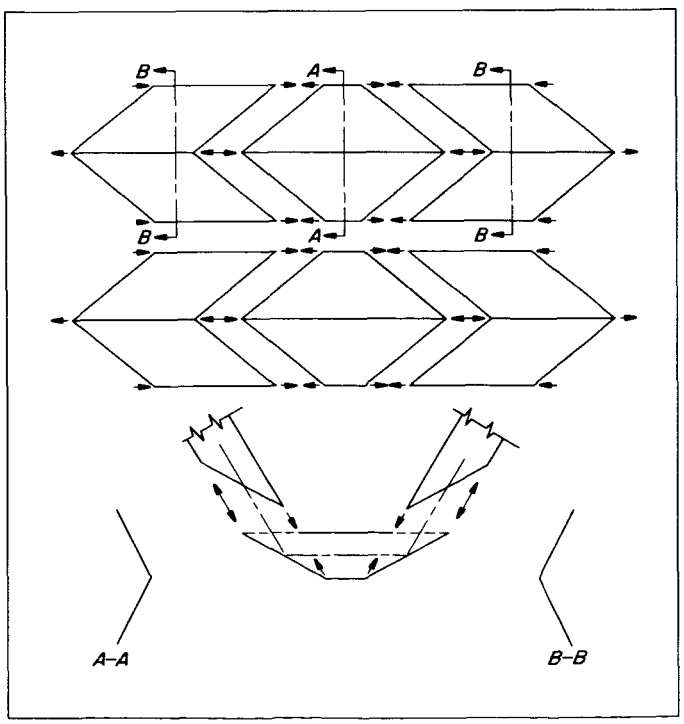

Fig. 8. Exploded view of cell model indicating forces causing in-plane deformation

Recalling the relations expressed in Eq. (1) through (5) and (10), the shear deformation energy is computed in the following manner. Referring to Fig. 9, replacing the forces shown by equivalent shear forces, an expression can then be formulated for energy of deformation in terms of the shear yield stress. Hence,

$$dU_2 = q_{yp}\, t\, (2\, B_t \sin\psi + 2A)\, d_2 \qquad (19)$$

Performing the necessary substitutions,

$$dU_2 = q_{yp}\, t \left[P_w \beta \sin\psi + D - \sqrt{3}\, P_w \sin\theta \right] \frac{2B_t}{\cos\psi}\, d\psi$$

and

$$dU_2 = q_{yp}\, \frac{t\, P_w^2\, d\psi}{K \cos^2\psi}$$

Since this value is for a configuration consisting of two basic panel elements, the energy increment per basic panel is

$$dU_2 = \frac{q_{yp}\, t\, P_w^2}{2\, K \cos^2\psi}\, d\psi \qquad (20)$$

As previously discussed, the integration is performed over two ranges of ψ, namely,

$$\psi = 0 \text{ deg} \quad \text{to } \psi = 40.89 \text{ deg}$$

$$\psi = 40.89 \text{ deg} \quad \text{to } \psi = 60 \text{ deg}$$

The basic panel elements must be formed before the shear deformation mechanism can occur. This requires that bending deformation mechanisms exist in the structure which define the basic panel elements before any energy will be absorbed in deforming these panels in shear. For rotations of $\psi = 0$ deg to $\psi = 40.89$ deg, the basic collapse mode is not clearly defined. Rotations occur but are not large enough to form definite panel elements. Thus, the deformation resulting from this rotation can occur without the presence of a shear mechanism.

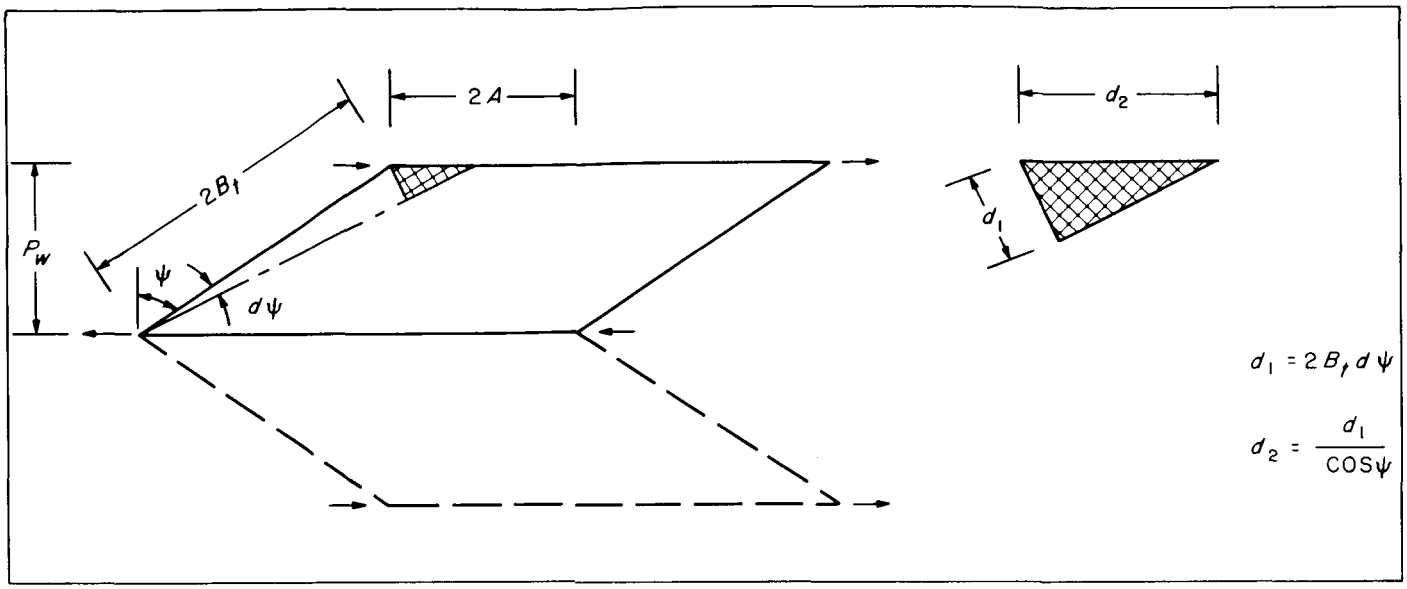

Fig. 9. Shear mechanism and corresponding parameters

This occurrence would not follow for a true rigid-plastic material; however, because of the interaction of the two deformation mechanisms, it is necessary to consider this deviation from a rigid-plastic material to better represent the collapse mechanisms that occur in an actual specimen. Therefore, integrating the shear energy expression over only the range of $\psi = 40.89$ deg to $\psi = 60$ deg,

$$U_2 = 0.433\, q_{yp} \frac{t P_w^2}{K} \tag{21}$$

Equating this expression to the change in potential energy of the applied force

$$U_2 = 0.433\, q_{yp} \frac{t P_w^2}{K} = f P_w$$

or

$$f = 0.433\, q_{yp} \frac{t P_w}{K}$$

The preceding expression represents the mean crushing force, and to convert this to the mean crushing stress, divide by the contributing area over which the force f acts:

$$F = 0.433\, q_{yp} \frac{t P_w}{K} \cdot \frac{8}{3\sqrt{3}D^2} = 1.155\, q_{yp} \frac{t}{S} \tag{22}$$

V. DISCUSSION OF RESULTS

If Eq. (18) and (22) are combined, an expression representing the mean crushing stress of a hexagonal cell structure is obtained:

$$F = \sigma_{yp} \frac{t^2}{S^2}\left[\frac{4.750}{K} + 28.628\right] + 1.155\, q_{yp} \frac{t}{S} \quad (23)$$

The parameters that govern Eq. (23) are the properties of the material from which the cell structure is fabricated and the structural density of the cellular array. The material properties are represented by the yield strength in bending and in shear. The density of the cell structure is a function of the term t/S which is the ratio of the cell wall thickness to the minor diameter of the cell. Thus, for a given cell diameter, the greater the wall thickness, the greater the crushing stress. One additional parameter occurs in Eq. (23), the term K. This term represents the ratio of one-fourth of a buckling wavelength to the width of a cell wall. In the process of crushing, the phenomenon of buckling as commonly accepted does not occur. The crushing process is one of progressive collapse. Only during initial loading does a specimen become unstable and buckle, and this occurs for the first panel fold only. However, in crushing, the specimen continues to collapse in this same manner with the same panel depth as the first buckled panel. Based upon classical theory, the approximate value of K is 0.50; however, it has been found that for the hexagonal cell structure, this value is very close to 0.40 for a wide range of t/S values.

The mean crushing stress as a function of t/S is plotted in Fig. 10, which indicates the lack of sensitivity of Eq. (23) to variations in K. For a $\pm 12\frac{1}{2}\%$ change in K, a change of approximately $\pm 4\%$ in mean crushing stress occurs; therefore, the mean crushing stress of a hexagonal cell structure is controlled, essentially, by the material properties and the structural density of the cellular array.

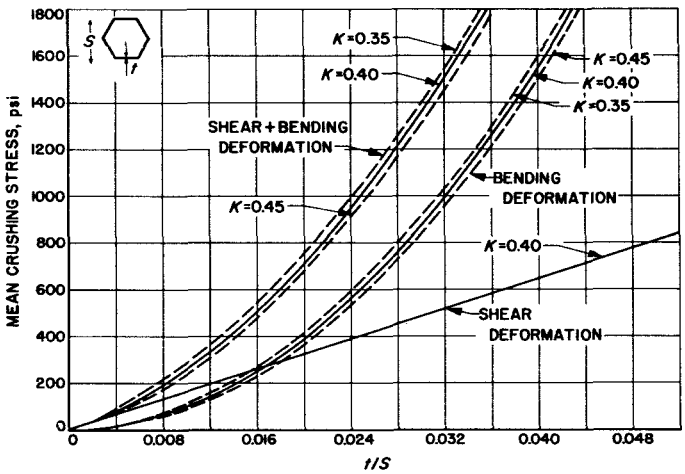

Fig. 10. Crushing stress vs. t/S for 3003 H-19 aluminum hexagonal cell structure

VI. EXPERIMENTAL RESULTS

To obtain experimental confirmation of the preceding analysis, test data were obtained for commercially available hexagonal cell structures of 0.016 maximum density (i.e., t/S).* To supplement these data, a number of cell structures were fabricated from 3003 H-19 aluminum alloy with a minor cell diameter of 0.75 in. The wall thickness of the cell structure was varied to give t/S ratios in the range of presently available structures and in excess of this range. Procedures used to obtain these data are discussed in the Appendix. The results of the experimental program plus data taken from published reports are shown in Fig. 11. The results indicate a good upper-bound correlation for t/S values up to 0.016.

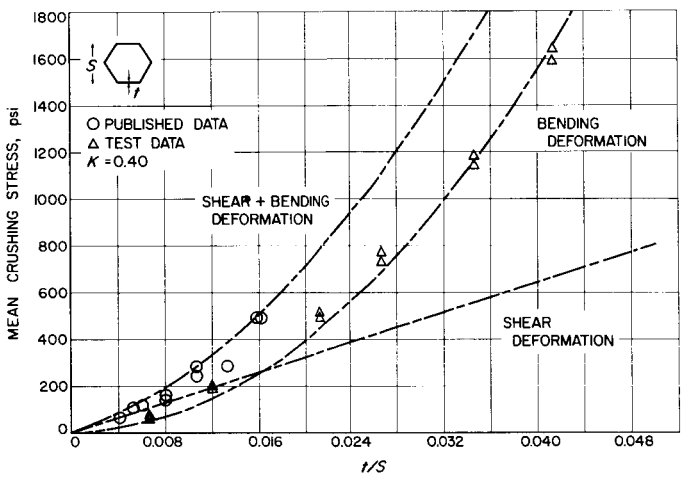

Fig. 11. Crushing stress vs. t/S for 3003 H-19 aluminum hexagonal cell structure

Data obtained from the test specimens indicate that the shear deformation energy is less than that assumed, particularly for increased values of t/S. The curve of bending deformation energy (Fig. 11), provides an effective lower bound for the mean crushing stress. It is apparent from Fig. 11 that the test data are consistently lower in value than published data. This, in part, is due to a scaling effect. The specimens tested consisted of approximately square arrays of 78 cells with five partially unsupported cells on two sides of each specimen (Fig. 1). Thus, in these arrays, 12.8% of the cells were not constrained in the same manner as interior cells. If specimens with exterior dimensions twice the size of those tested had been used, only 6.8% of the cells in the array would have been partially constrained. No attempt was made to evaluate the magnitude of this scaling factor, due to the apparently small effect it had on the total crushing stress. A limited amount of published test data were obtained for a 5052 H-39 aluminum hexagonal cell structure, shown in Fig. 12 along with the derived relations using the 5052 H-39 material properties.

Of additional interest, it was found that there is an upper limit on the t/S ratio at which the hexagonal cell structure will collapse in a mode of failure which is entirely different from the mode normally observed. This failure mode is essentially a gross shear failure, as shown in the two views in Fig. 13. The t/S ratio for the test specimen at which this mode of failure begins to appear under static loading is approximately 0.040. The energy absorption of the shear mode is less than would be obtained by the crushing mode previously considered for corresponding t/S ratios. The emergency of the shear mode is controlled by the material properties and the t/S ratio.

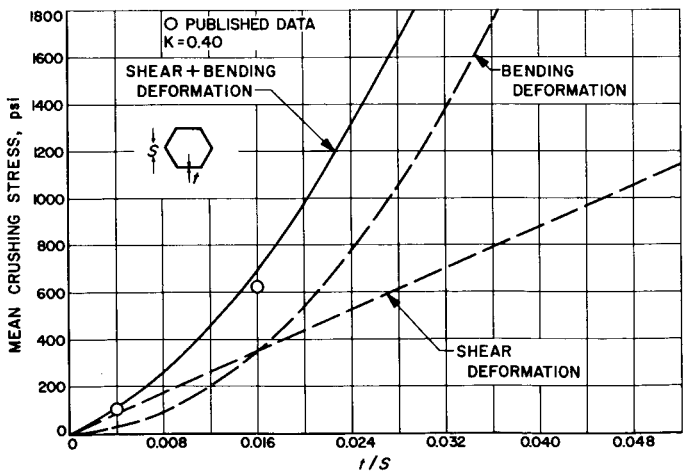

Fig. 12. Crushing stress vs. t/S for 5052 H-39 aluminum hexagonal cell structure

Energy Absorption Properties of Aluminum Honeycomb, TSB-110, Hexcell Products, Inc., Berkeley, Calif., 1960

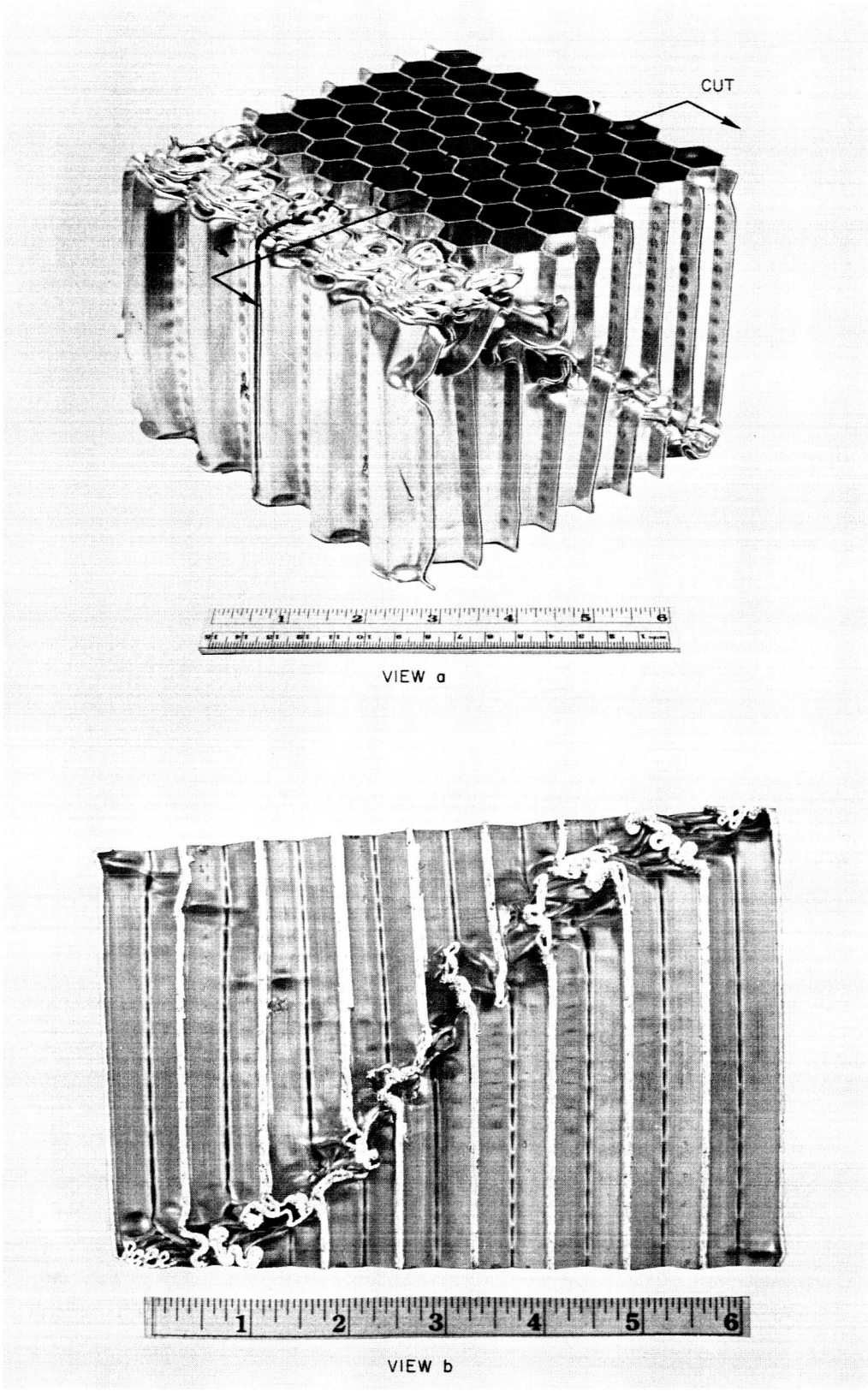

Fig. 13. Views of partially crushed hexagonal cell structure showing shear failure

VII. CONCLUSION

The foregoing analysis is presented as a first approach to the problem of determining the mean crushing stress of hexagonal cell structures. As previously stated, the purpose of this analysis was to derive a relationship for calculating the mean crushing stress and to determine the parameters that control it, with the end goal of providing a rational basis for the design of more efficient energy-absorbing structures. The method of analysis is a standard one, used to a large extent in structural analyses. There are a number of refinements to this theory, but no attempt was made to apply them due to the complex nature of the structure considered.

The results indicate a favorable correlation between theory and experiment for the limited amount of test data available. The use of higher yield stress materials, possessing adequate ductility, for the fabrication of the hexagonal cell structures would result in energy-absorbing properties well in excess of those exhibited by present-day aluminum-alloy cell structures.

NOMENCLATURE

A basic panel element dimension

B horizontal projection of basic panel element dimension

B_t true length of B

D width of cell wall

F mean crushing stress

f mean crushing force

K P_w/D

M_{yp} plastic moment per unit of length

P_w width of basic panel element

q_{yp} shear yield stress

S cell minor diameter

t cell wall thickness

U energy

β $(1 + 3 \sin^2\theta)^{1/2}$

θ, ϕ angles representing degree of collapse of a single cell element

ψ angle representing shear deformation of a single cell element

σ_{yp} tensile yield stress

APPENDIX

Test Procedures

As an initial step in the experimental procedure, test results for hexagonal cell structures were obtained from various references (see Bibliography). Data available on this topic are very limited and the majority of the data are for hexagonal cell structures fabricated of 3003 H-19 aluminum. The maximum structural density (i.e., t/S) of cell structure presently commercially available, and for which data is available, is 0.016.

In order to extend the range of data, a number of hexagonal-cell structures were fabricated, using 3003 H-19 aluminum. Two specimens were fabricated for each of six different structural densities: .0067, .0120, .0213, .0267, .0347, and .0413. The cell minor diameter of all specimens was 0.75 in. The length of the specimens was approximately 6 in., and the cross-sectional dimensions 6.0 x 6.5 in. Figure A-1 shows a specimen prior to loading.

The specimens were fabricated by spot welding the plate elements together. This method was used in lieu of organic adhesives because of the heavier structural densities involved, and to develop means other than the use of adhesives for fabrication.

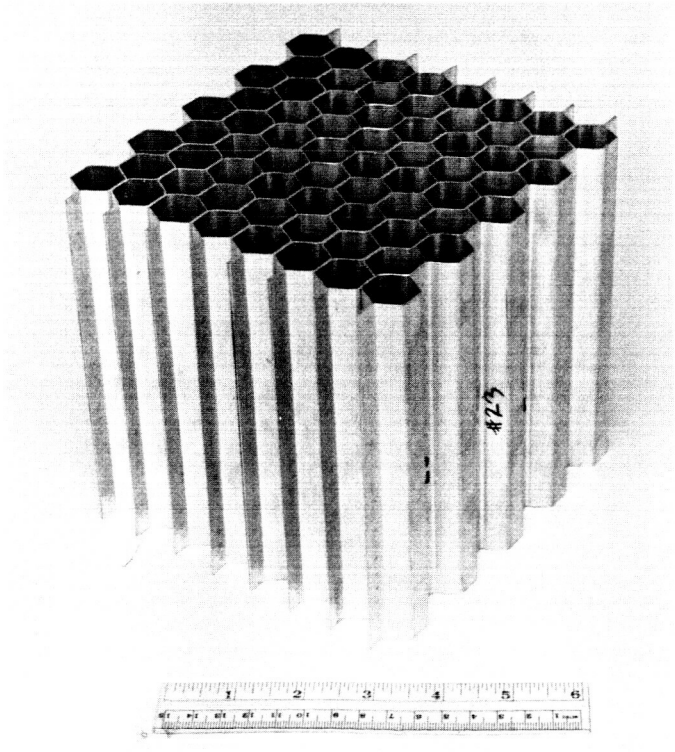

Fig. A-1. Hexagonal cell structure prior to testing

The testing procedure consisted of static loading in a Baldwin hydraulic testing machine, utilizing an automatic load-displacement plotter. The loading surfaces of the specimens were carefully ground to obtain plane surfaces perpendicular to the loading axis of the specimen. The tests were performed by loading the specimen directly through machined loading surfaces without the use of a spherical loading block. No attempt was made to minimize frictional constraints on the specimen at the loading surfaces, as buckling was always initiated a short distance away from either the top or bottom loading surface.

The result of a typical static compression test is shown in Fig. A-2. From this figure, it is noted that the initial peak buckling load is followed by a relatively uniform progressive collapse of the specimen. Figure 1b (Part II) is a photograph of a cut taken through a partially collapsed specimen, showing the uniformity of the collapse mode.

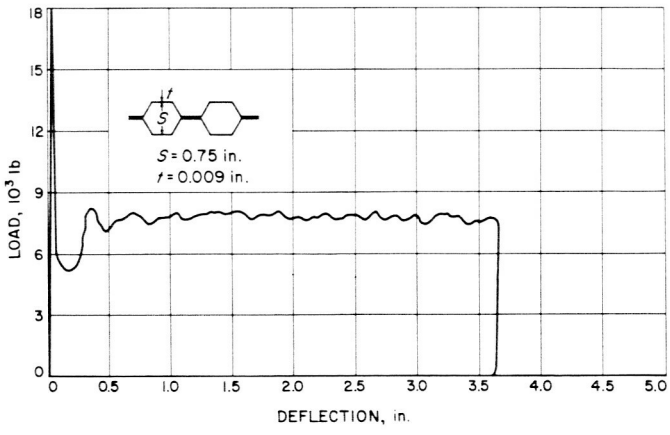

Fig. A-2. Load-deflection curve for 3003 H-19 aluminum hexagonal cell structure loaded statically

In addition to the testing of the above-mentioned specimen, several 6-in.-diam. hexagonal cells were fabricated. These specimens were coated with brittle lacquer and loaded axially to observe the formation of yield mechanisms during the collapse of the specimen. As previously

stated, the mode of collapse of a single hexagonal cell is different from the collapse mode of a hexagonal cell structure; however, the difference is one of symmetry only. The single hexagonal cell collapses in a mode which is symmetric on all sides, whereas the hexagonal cell in a cellular array collapses in a mode which is symmetric and antisymmetric alternatively around the cell. As a result of the similarity of the modes, the absence of the in-plane shear mechanism in the symmetric sides for the two modes could be verified.

BIBLIOGRAPHY

Alexander, J. M., "An Approximate Analysis of the Collapse of Thin Cylindrical Shells Under Axial Loading," *Quarterly Journal of Mechanics and Applied Mathematics*, Vol. XIII, Part I, 1960.

O'Bryan, T. C. and Hatch, H. G., *Limited Investigation of Crushable Structures for Acceleration Protection of Occupants of Vehicles at Low Impact Speeds*, TN D-158, National Aeronautics and Space Administration, Washington, D. C., October 1959.

Pugsley, A. and Macaulay, M., "The Large-Scale Crumpling of Thin Cylindrical Columns," *Quarterly Journal of Mechanics and Applied Mathematics*, Vol. XIII, Part I, 1960.

Radioplane, *Impact Deceleration Systems Applicable to Lunar Landing Vehicles*, Report No. 2324, Van Nuys, Calif., 1960.

University of Texas, *Cushioning for Air Prop — Part I*, Structural Mechanics Research Laboratory, Austin, July 1955.

University of Texas, *Cushioning for Air Drop — Part III*, Structural Mechanics Research Laboratory, Austin, August 1956.

University of Texas, *Cushioning for Air Drop — Part VIII*, Structural Mechanics Research Laboratory, Austin, June 1957.

University of Texas, *Cushioning for Air Drop — Part IX*, Structural Mechanics Research Laboratory, Austin, June 1957.

University of Texas, *High Velocity Impact Cushioning — Part II*, Structural Mechanics Research Laboratory, Austin, August 1957.